
Article:
Bryan, M.T., Fry, P.W., Schrefl, T. et al. (4 more authors) (2010) Transverse field-induced nucleation pad switching modes during domain wall injection. IEEE Transactions on Magnetics, 46 (4). pp. 963-967. ISSN 0018-9464

https://doi.org/10.1109/TMAG.2009.2034848

Transverse Field-Induced Nucleation Pad Switching Modes During Domain Wall Injection

Matthew T. Bryan[1], Paul W. Fry[2], Thomas Schrefl[1,3], Mike R. J. Gibbs[1], Dan A. Allwood[1], Mi-Young Im[4], and Peter Fischer[4]

[1]Department of Engineering Materials, University of Sheffield, Sheffield S1 3JD, U.K.
[2]Nanoscience and Technology Centre, University of Sheffield, Sheffield S3 7HQ, U.K.
[3]St. Poelten University of Applied Sciences, 3100 St. Poelten, Austria
[4]LBNL/CXRO, Berkeley, CA 94720 USA

We have used magnetic transmission soft X-ray microscopy (M-TXM) to image in-field magnetization configurations of patterned $Ni_{80}Fe_{20}$ domain wall "nucleation pads" with attached planar nanowires. Comparison with micromagnetic simulations suggests that the evolution of magnetic domains in rectangular injection pads depends on the relative orientation of closure domains in the remanent state. The magnetization reversal pathway is altered by the inclusion of transverse magnetic fields. These different modes explain previous results of domain wall injection into nanowires.

Index Terms—**Domain wall injection, nanowires, nucleation pad, switching modes, transverse field.**

I. Introduction

MAGNETIZATION reversal in simple, straight nanowires usually occurs via domain wall nucleation and propagation from one end (or both ends) of the wire [1], [2]. The switching of the nanowire can be significantly reduced if a large, magnetically soft pad is fabricated on one of the wire ends [3]–[5]. These "nucleation pads" reverse at lower fields than a typical isolated nanowire and hence introduce a domain wall to the wire from the wire end attached to the pad. Domain walls nucleated in a pad often become pinned at the pad/wire junction [3], [4], [6], [7], so they cannot be introduced into the wire until a critical "injection" field is reached. Once this occurs, the domain wall sweeps through the wire, reversing its magnetization. The injection field is designed to be lower than the nucleation field without a pad so that devices can be tested without unwanted domain wall nucleation, or device breakdown, occurring [8]–[10]. Nucleation pads are, therefore, a simple and convenient way of introducing domain walls with a clearly defined propagation direction to sometimes complex devices at low fields. Carefully designed nucleation pads can also be used to control the chirality of injected vortex domain walls [11]. Nucleation pads vary widely in dimensions and shape, with squares, circles, ellipses, rectangles, and several irregular shapes being investigated [3]–[5], [11], [12]. More than one remanent magnetic domain configuration, or mode, can be observed within a pad after successive domain wall injections, with each mode resulting in a particular injection field [13].

Nucleation pads are frequently used as part of nanowire devices and experimental structures. Magnetic-field-driven shift register memory can include an nucleation pad to write data [14] while those attached to nanowire spiral turn sensors act as both a source and sink of domain walls [15]. Both of these devices use 2-D wire circuits and therefore require the use of orthogonal in-plane magnetic fields to drive domain walls through wires of different orientations. These biaxial fields can significantly alter the fields at which domain wall injection occurs, control the number of injection modes that exist with attached wires of various widths [16], and influence the domain wall chirality [17], [18]. Multimodal behavior, observed in single-shot hysteresis loops as a stochastic variation of axial injection fields between particular values, only occurred below a critical transverse field. However, the mechanism behind this behavior has not been established.

Here, we image by high resolution magnetic transmission soft X-ray microscopy (M-TXM) the evolution of magnetic domains during field-driven reversal of nucleation pads and observe the resulting domain wall injection in attached wires. Comparing the magnetic configuration of the nucleation pads with micromagnetic models, we find that the relative orientation of closure domains in the remanent magnetization configuration of nucleation pads determines the reversal pathway that follows, although this is further affected by applied transverse fields.

II. Experimental Setup

24-nm-thick thermally evaporated $Ni_{80}Fe_{20}$ (permalloy) structures were fabricated on 100 nm thin Si_3N_4 membranes using electron beam lithography followed by lift-off in acetone. The structures consisted of $2\ \mu m \times 3\ \mu m$ nucleation pads with wires of width 200 nm, 300 nm, or 500 nm attached (Fig. 1). The 180° arc in the wire was not used in this experiment and is not expected to influence the injection modes of the pad. Fig. 1 also defines the orthogonal x and y directions, along which the fields H_x and H_y are applied, respectively.

Magnetic transmission X-ray microscopy (M-TXM) was performed at beamline 6.1.2 at the Center for X-ray Optics, Advanced Light Source, Berkeley, CA [19]. Magnetization contrast in M-TXM images is due to the differential absorption of circularly polarized X-rays in magnetic materials due to X-ray

Manuscript received August 03, 2009; accepted October 08, 2009. First published November 03, 2009; current version published March 19, 2010. Corresponding author: M. T. Bryan (e-mail: m.t.bryan@shef.ac.uk).

Color versions of one or more of the figures in this paper are available online at http://ieeexplore.ieee.org.

Digital Object Identifier 10.1109/TMAG.2009.2034848

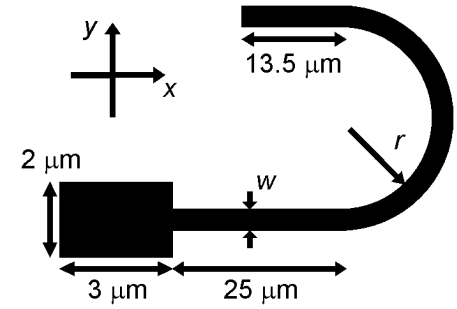

Fig. 1. Schematic diagram of the structures studied. Wires have width $w = 200$ nm, 300 nm, or 500 nm and a 180° arc of radius, $r = 2$ μm when $w = 200$ nm or 300 nm, and $r = 4$ μm when $w = 500$ nm.

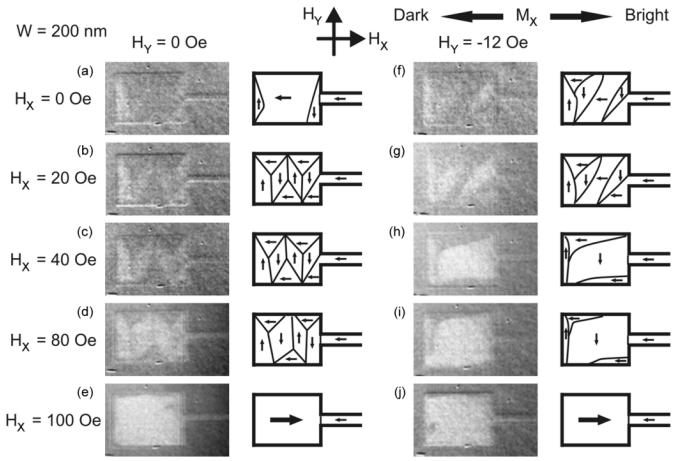

Fig. 2. M-TXM images showing the magnetization state of a nucleation pad with a 200-nm-wide wire under fields H_x and H_y. The schematics are a guide to aid interpretation of the images. The reference image is at saturation under $H_x = -500$ Oe.

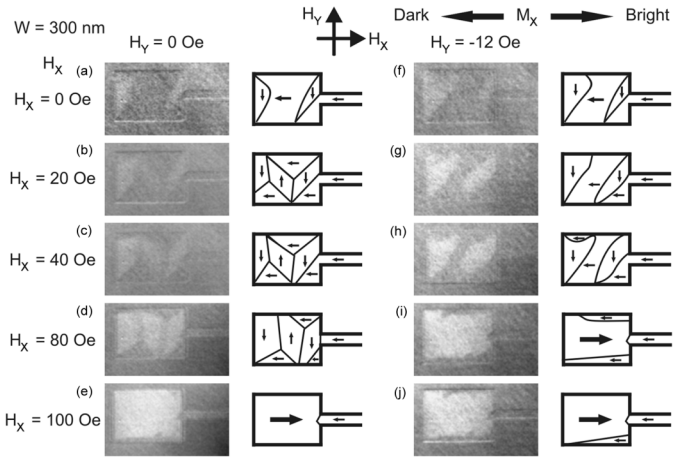

Fig. 3. M-TXM images showing the magnetization state of a nucleation pad with a 300-nm-wide wire under fields H_x and H_y. The schematics are a guide to aid interpretation of the images. The reference image is at saturation under $H_x = -500$ Oe.

magnetic circular dichroism (X-MCD). As the technique is only sensitive to magnetization components along the X-ray optical axis, the structures are held at an angle of 30° to the optical axis to provide contrast in the x-direction. The X-rays are focused using Fresnel zone plates to provide better than 25 nm spatial resolution with an approximately 10 μm field of view on an X-ray sensitive charge-coupled device camera. Together with a 12 μm diameter pinhole, the zone plates also act as a linear monochromator, enabling the X-ray photon energy to be selected at either 706 eV or 853 eV in order to be sensitive to the Fe or Ni L_3-edges. Electromagnets are used to apply fields H_x and H_y during and between image capture. The signal-to-noise ratio of raw images is improved by averaging several images from the CCD camera, binning adjacent CCD pixels and applying digital smoothing functions. The images shown here are obtained by dividing two raw images obtained under different field conditions to show changes in magnetization and remove the strong contrast between regions containing magnetic structure and bare substrate. One image (the "reference" image) is taken under saturation conditions, so the final images shown represent the magnetization state of the second raw image. Full details of the experimental arrangement of the microscope can be found elsewhere [20], [21].

Micromagnetic simulations were performed using a hybrid finite element/boundary element code to solve the Landau–Lifshitz–Gilbert equation of motion [22], [23] that has previously been used to solve magnetization dynamics of domain walls in magnetic nanowires [24], [25]. The modeled structure consisted of a 2 μm × 3 μm pad wire a 500-nm-wide, 2-μm-long wire attached, mimicking the essential features of the experimental structures. The thickness of the simulated structures and the maximum cell size is 20 nm. Edge roughness was not included in the model as it is unlikely to affect the domain structure of the pad. The material properties of bulk permalloy were used in the model, with exchange stiffness $A = 1.3 \times 10^{-11}$ J/m, saturation magnetization $M_S = 800$ kA/m, magneto-crystaline anisotropy $K = 0$ Jm^{-3} and damping constant $\alpha = 0.01$. The injection field was found by linearly increasing the axial magnetic field at a rate of 1 Oe/ns until the domain wall entered the wire.

III. Results and Discussion

Figs. 2–5 show M-TXM images of nucleation pads and 200-nm, 300-nm, and 500-nm-wide wires under various H_x and H_y. Note that $H_x \geq 0$ Oe and $H_y \leq 0$ Oe in Figs. 2 and 3, but $H_x \leq 0$ Oe and $H_y \geq 0$ Oe in Figs. 4 and 5. Also, Figs. 3 and 4 show two nominally identical structures, not the same structure. In all the structures, the remanent magnetization state of the pad with no transverse field (part (a) of Figs. 2–5) consists of a uniform magnetization aligned with the wire axis, with closure domains at the edges facing and joining the wire. When $H_y = 0$ Oe and $H_x = 20$ Oe, the magnetization state of the pad buckles, forming either eight [Figs. 2(b) and 5(b)] or six [Figs. 3(b) and 4(b)] domains, half of which have magnetizations rotated away from the x-axis. As H_x is increased, the rotation of the domains become larger and the nonrotated domains shrink [Figs. 2(a)–(d), 3(a)–(d), 4(a)–(d), and 5(a)–(d)]. By $|H_x| = 100$ Oe (125 Oe for the 500-nm-wide wire), the magnetization in each pad is aligned with the field, and a domain wall is either left at the junction with the wire [Figs. 2(e) and 3(e)], or injected into the wire [Figs. 4(e) and 5(e)].

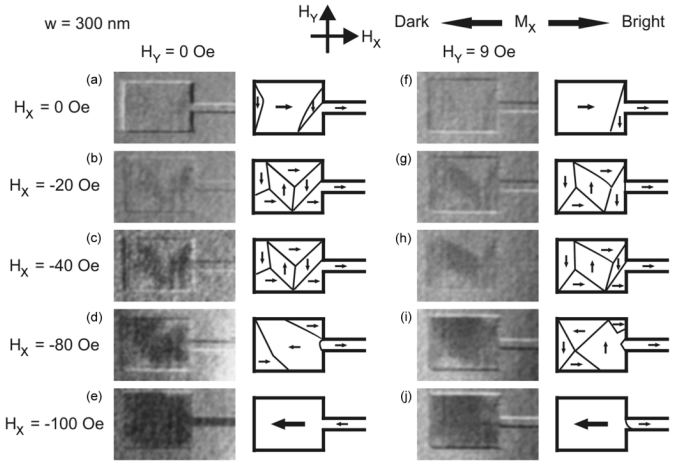

Fig. 4. M-TXM images showing the magnetization state of a nucleation pad with a 300-nm-wide wire under fields H_x and H_y. The schematics are a guide to aid interpretation of the images. The reference image is at saturation under $H_x = 500$ Oe.

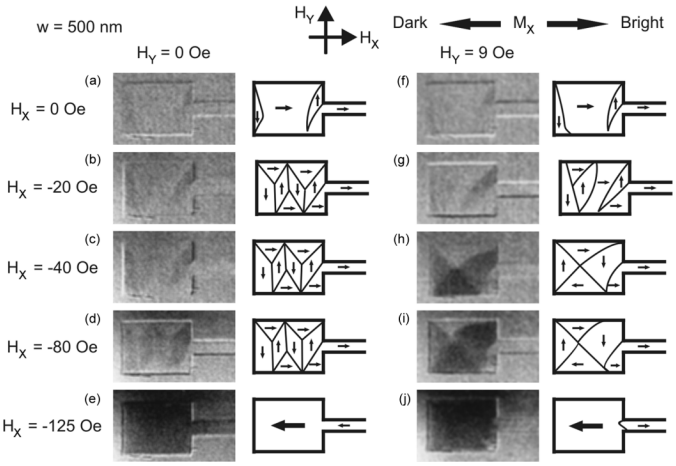

Fig. 5. M-TXM images showing the magnetization state of a nucleation pad with a 500-nm-wide wire under fields H_x and H_y. The schematics are a guide to aid interpretation of the images. The reference image is at saturation under $H_x = 500$ Oe.

When the magnetization of the pad is reset and a transverse field is applied in addition to the axial field, more complex modes of magnetization reversal are seen in the pad. In the pad with the 200-nm-wide wire under $H_y = -12$ Oe [Figs. 2(f)–(j)], the magnetization enters a six-domain state when $H_x \leq 20$ Oe [Fig. 2(f) and (g)], but changes into a four-domain state at $H_x = 40$ Oe [Fig. 2(h) and (i)], before the pad completes magnetization reversal at $H_x \sim 100$ Oe [Fig. 2(j). The magnetization states of the pads with 300-nm-wide wires under a transverse field [Figs. 3(f)–(j) and 4(f)–(j)] appear to be distorted forms of the magnetization state with no transverse field when $|H_x| \leq 40$ Oe. However, these low field distortions are complements of each other: in one pad wire closure domains are expanded and the central domain is reduced [Figs. 3(f)–(h)], whereas in the other wire the closure domains are reduced and the central domain is expanded [Figs. 4(f)–(h)]. These distortions precede differences in the ongoing evolution of magnetization, with the former pad undergoing almost complete reversal between $|H_x| = 80$–100 Oe [Figs. 3(i) and (j)] while the latter forms a Landau pattern, or vortex, at $|H_x| = -80$ Oe [Fig. 4(i)] that is expelled at higher fields to complete the magnetization reversal [Fig. 4(j)]. The pad with a 500-nm-wide wire under $H_y = 9$ Oe forms a six-domain state when $|H_x| \leq 20$ Oe [Figs. 5(f) and (g)], but this changes to a vortex state at higher fields [Figs. 5(h) and (i)]. The vortex is gradually driven out of the pad as H_x is increased, until a uniform magnetization state is reached at $|H_x| = 125$ Oe [Fig. 5(j)].

While we have not studied the effect of wire width on the magnetization state of the pad comprehensively, similar magnetization states were observed in pads with different width wires attached. For example, Figs. 2(b) and 5(b) show similar magnetization configurations in pads with 200-nm and 500-nm-wide wires attached, respectively, while Figs. 2(f)–(j) and 3(f)–(j), and Figs. 4(f)–(j) and 5(f)–(j) each show very similar magnetization reversal pathways under transverse fields. This suggests that the different magnetization states seen are alternative modes of pad reversal that are independent of the wire width, rather than an effect of the wire width on the shape anisotropy at the pad-wire junction. This stochastic behavior has been previously observed in different shaped pads [13], where the number of modes present was temperature-dependent.

Although the transverse field affects the mode of reversal in the pad, ultimately the pad reaches a single-domain magnetization before a domain wall is injected into the wire [part (j) of Figs. 2–5]. Nevertheless, the transverse field does appear to influence domain wall injection. For example, the 500-nm-wide wire switched at $H_x = -125$ Oe without a transverse field, but at $H_x = -130$ Oe when $H_y = 9$ Oe. This increase in domain wall injection field resulting from the inclusion of transverse fields contrasts with our previous results from pads and wires of different dimensions [16]. This indicates that the detailed effect of transverse field is likely to depend on the particular pad/wire geometry and dimensions employed and does not follow a generic rule.

We have been able to understand the pathway of pad magnetization more generally by using micromagnetic simulations. Fig. 6 shows the micromagnetically calculated magnetization structures under fields $H_x = 15$ Oe and $H_y = 0$ Oe and ± 10 Oe. Two initial configurations are shown, with the closure domain on the left-hand edge of the pad either parallel [Fig. 6(a)] or anti-parallel [Fig. 6(b)] to both closure domains on the right-hand edges of the pad. A third configuration was also modeled, with the closure domains on the right-hand edge opposing each other, but this had a higher energy than the other two configurations and behaved in a similar way to that shown Fig. 6(b), so will be neglected from the following analysis. The alignment of the closure domains determines the number of domains that form within the pad. Where all the closure domains are aligned [Fig. 6(a) ii], the simulations accurately reproduce the six-domain magnetization patterns seen experimentally with the 300-nm-wide wires and no transverse field [Figs. 3(b) and 4(b)]. Comparison of the M-TXM images and the micromagnetic modeling suggests that magnetization states that occur in the pads with the 300-nm-wide wires under a transverse field [Figs. 3(g) and 4(g)] have closure domains that

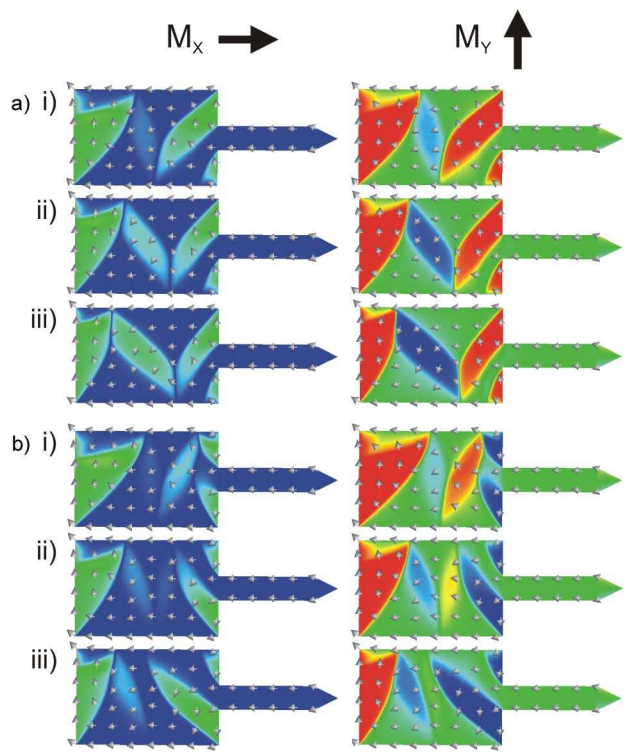

Fig. 6. Micromagnetic simulations of a pad attached to a 500-nm-wide wire. The closure domains on the right-hand side of the pad are (a) parallel or (b) anti-parallel to the left-hand closure domain. In each case, $H_x = 15$ Oe and $H_y = (i)$ 10 Oe, (ii) 0 Oe, and (iii) -10 Oe.

are aligned. The ensuing magnetization reversal pathways differ because the transverse field is parallel to the closure domains in Fig. 3(g) [similar to Fig. 6(a) i] and anti-parallel to the closure domains in Fig. 4(g) [similar to Fig. 6(a) iii]. In the absence of a transverse field, an eight-domain magnetization state in the pads is predicted by the models when the closure domains on the right-hand edges are both anti-parallel to the closure domain on the left-hand edge [Fig. 6(b) ii]. This is similar to those seen experimentally in Figs. 2(b) and 5(b). Under $H_y = -10$ Oe [Fig. 6(b) iii], the domains rotate to form a state similar to those observed in Figs. 2(g) and 5(g). We can predict, therefore, that the magnetization reversal pathway in square or rectangular nucleation pads depends primarily on the relative orientation of closure domains. In our M-TXM experiments, the transverse fields were only applied after the remanent state had been reached with an axial field. Our previous experiments [16] used a continuously rotating magnetic field. For domain wall injection into narrow wires, bimodal behavior tended to cease as the transverse field component increased. It is now clear that this may have been due to the transverse field aligning opposite closure domains, thus dictating the subsequent magnetization reversal pathway.

As H_x was increased in the calculations to inject a domain wall, the pad magnetization states changed from those shown in Fig. 6 to vortex states, as observed by M-TXM in pads with a 500-nm-wide wire attached [Fig. 5(h)]. At higher fields, the magnetization of the modeled pad became single-domain, although closure domains remained at fields up to $H_x = 90$ Oe. Different injection fields were observed with pads of different initial closure domain configurations when no transverse field was applied. Pads initially magnetized with parallel closure domains injected domain walls at $H_x = 59$ Oe, 45 Oe, or 44 Oe when $H_y = 10$ Oe, 0 Oe, or -10 Oe, respectively. By contrast, when the closure domains of the pad were anti-parallel, domain walls were injected at $H_x = 56$ Oe, 56 Oe, or 54 Oe while $H_y = 10$ Oe, 0 Oe, or -10 Oe, respectively. The increase in injection field for the parallel case when $H_y = 10$ Oe was brought about by a reversal in the closure domain configuration so that, at the point of injection, they had become anti-parallel. Therefore, the model predicts two injection modes, one at around 45 Oe due to parallel closure domains and another at around 56 Oe due to anti-parallel closure domains. This supports the suggestion that experimentally observed multimodal injection is due to the magnetization state of the pad [13], [16]. Interestingly, the lowest energy state prior to injection occurs when the closure domains are parallel. As the lowest injection field occurs in this state, this indicates that the injection field is determined mainly by the localized reversal mode, rather than minimization of the global energy of the system.

IV. Conclusion

We have used micromagnetic simulation and magnetic transmission soft X-ray microscopy (M-TXM) providing 25 nm spatial resolution to investigate the evolution of magnetization configurations in patterned $Ni_{80}Fe_{20}$ rectangular nucleation pads and attached wires during domain wall injection. The relative orientation of closure domains in the pads determines the magnetization reversal pathway under an axial field. However, the addition of a transverse field can alter the closure domain configuration, affecting the axial field at which domain walls are injected.

Acknowledgment

This work was supported by EPSRC under Grants GR/T02959/01 and EP/D056683/1, by a EPSRC DTA studentship, and by the Director, Office of Science, Office of Basic Energy Sciences, Materials Sciences and Engineering Division, U.S. Department of Energy.

References

[1] T. Schrefl, J. Fidler, K. J. Kirk, and J. N. Chapman, "Domain structures and switching mechanisms in patterned magnetic elements," *J. Magn. Magn. Mater.*, vol. 175, p. 193, 1997.
[2] R. Ferre, "Magnetization reversal in finite and infinite square prisms," *Comput. Mater. Sci.*, vol. 10, p. 278, 1998.
[3] K. Shigeto, T. Shinjo, and T. Ono, "Injection of a magnetic domain wall into a submicron magnetic wire," *Appl. Phys. Lett.*, vol. 75, p. 2815, 1999.
[4] R. P. Cowburn, D. A. Allwood, G. Xiong, and M. D. Cooke, "Domain wall injection and propagation in planar Permalloy nanowires," *J. Appl. Phys.*, vol. 91, p. 6949, 2002.
[5] A. Yamaguchi, S. Nasu, H. Tanigawa, T. Ono, K. Miyake, K. Mibu, and T. Shinjo, "Effect of Joule heating in current-driven domain wall motion," *Appl. Phys. Lett.*, vol. 86, p. 012511, 2005.
[6] M. Brands and G. Dumpich, "Multiple switching fields and domain wall pinning in single Co domains," *J. Phys. D Appl. Phys.*, vol. 38, p. 822, 2005.

[7] L. Thomas, C. T. Rettner, M. Hayashi, M. Samant, S. S. P. Parkin, A. Doran, and A. Scholl, "Observation of injection and pinning of domain walls in magnetic nanowires using photoemission electron microscopy," *Appl. Phys. Lett.*, vol. 87, p. 262501, 2005.

[8] C. C. Faulkner, D. A. Allwood, M. D. Cooke, G. Xiong, D. Atkinson, and R. P. Cowburn, "Controlled switching of ferromagnetic wire junctions by domain wall injection," *IEEE Trans. Magn.*, vol. 39, no. 5, pp. 2860–2862, Sep. 2003.

[9] C. C. Faulkner, M. D. Cooke, D. A. Allwood, D. Petit, D. Atkinson, and R. P. Cowburn, "Artificial domain wall nanotraps in $\mathrm{Ni_{81}Fe_{19}}$ wires," *J. Appl. Phys.*, vol. 95, p. 6717, 2004.

[10] D. A. Allwood, G. Xiong, and R. P. Cowburn, "Domain wall cloning in magnetic nanowires," *J. Appl. Phys.*, vol. 101, p. 024308, 2007.

[11] D. McGrouther, S. McVitie, J. N. Chapman, and A. Gentils, "Controlled domain wall injection into ferromagnetic nanowires from an optimized pad geometry," *Appl. Phys. Lett.*, vol. 91, p. 022506, 2007.

[12] K. Shigeto, T. Okuno, T. Shinjo, Y. Suzuki, and T. Ono, "Magnetization switching of a magnetic wire with trilayer structure using giant magnetoresistance effect," *J. Appl. Phys.*, vol. 88, p. 6636, 2000.

[13] K. Shigeto, K. Miyake, T. Okuno, K. Mibu, T. Ono, Y. Yokoyama, T. Kawagoe, Y. Suzuki, and T. Shinjo, "Temperature dependence of switching field distribution in a NiFe wire with a pad," *J. Magn. Magn. Mater.*, vol. 240, p. 301, 2002.

[14] D. A. Allwood, G. Xiong, and R. P. Cowburn, "Writing and erasing data in magnetic domain wall logic systems," *J. Appl. Phys.*, vol. 100, p. 123908, 2006.

[15] M. Diegel, R. Mattheis, and E. Halder, "Multiturn counter using movement and storage of 180° domain walls," *Sensor Lett.*, vol. 5, p. 118, 2007.

[16] M. T. Bryan, D. Atkinson, and D. A. Allwood, "Multimode switching induced by a transverse field in planar magnetic nanostructures," *Appl. Phys. Lett.*, vol. 88, p. 032505, 2006.

[17] D. Atkinson, D. S. Eastwood, and L. K. Bogart, "Controlling domain wall pinning in planar nanowires by selecting domain wall type and its application in a memory concept," *Appl. Phys. Lett.*, vol. 92, p. 022510, 2008.

[18] A. Kunz and S. C. Reiff, "Dependence of domain wall structure for low field injection into magnetic nanowires," *Appl. Phys. Lett.*, vol. 94, p. 192504, 2009.

[19] [Online]. Available: http://www.cxro.lbl.gov/BL612/

[20] P. Fischer, D. H. Kim, W. Chao, J. A. Liddle, E. H. Anderson, and D. T. Attwood, "Soft X-ray microscopy of nanomagnetism," *Mater. Today*, vol. 9, p. 26, 2006.

[21] P. Fischer, "Studying nanoscale magnetism and us dynamics with soft-X-ray microscopy," *IEEE Trans. Magn.*, vol. 44, no. 7, pp. 1900–1902, Jul. 2008.

[22] D. R. Fredkin and T. R. Köhler, "Hybrid method for computing demagnetizing fields," *IEEE Trans. Magn.*, vol. 26, no. 2, pp. 415–417, Mar. 1990.

[23] D. Suess, V. Tsiantos, T. Schrefl, J. Fidler, W. Scholz, H. Forster, R. Dittrich, and J. Miles, "Time resolved micromagnetics using a preconditioned time integration method," *J. Magn. Magn. Mater.*, vol. 248, p. 298, 2002.

[24] M. T. Bryan, T. Schrefl, and D. A. Allwood, "Symmetric and asymmetric domain wall diodes in magnetic nanowires," *Appl. Phys. Lett.*, vol. 91, p. 142502, 2007.

[25] M. T. Bryan, T. Schrefl, D. Atkinson, and D. A. Allwood, "Magnetic domain wall propagation in nanowires under transverse magnetic fields," *J. Appl. Phys.*, vol. 103, p. 073906, 2008.